NUMERICAL STUDY OF FREE CONVECTIVE MHD FLOW PAST A VERTICAL CONE IN NON-DARCIAN POROUS MEDIA

S.Gouse Mohiddin   **O.Anwar Bég**
S.Vijaya Kumar Varma

Numerical study of free convective MHD flow past a vertical cone in non-darcian porous media

S.Gouse Mohiddin*   O.Anwar Bég [†]

S.Vijaya Kumar Varma[‡]

Abstract

A numerical study of buoyancy-driven unsteady natural convection boundary layer flow past a vertical cone embedded in a non-Darcian isotropic porous regime with transverse magnetic field applied normal to the surface is considered. The heat and mass flux at the surface of the cone is modeled as a power-law according to $q_w(x) = x^m$ and $q_w^*(x) = x^n$ respectively, where x denotes the coordinate along the slant face of the cone. Both Darcian drag and Forchheimer quadratic porous impedance are incorporated into the two-dimensional viscous flow model. The transient boundary layer equations are then non-dimensionalized and solved by the Crank-Nicolson implicit difference method. The velocity, temperature and concentration fields have been studied for the effect of Grashof number, Darcy number, Forchheimer number, Prandtl number, surface heat flux power-law exponent (m), surface mass flux power-law exponent (n), Schmidt number, buoyancy ratio parameter and semi-vertical angle of the cone. Present results for selected variables for the purely fluid regime are compared with the non-porous study by Hossain and Paul [9] and are found to be in excellent agreement. The local skin friction, Nusselt number and Sherwood number are also analyzed graphically. The study finds important applications in geophysical heat transfer, industrial manufacturing processes and hybrid solar energy systems.

Keywords: cone, non-Darcian porous media, finite difference method, heat mass flux.

*Department of Mathematics, Madanapalle Institute of Technology Science, Madanapalle-517325, AP, India, e-mail: gousemaths@gmail.com

[†]Biomechanics and Biotechnology Research, Aerospace Engineering Program, Mechanical Engineering Subject Group, Sheaf Building, Sheffield Hallam University, Sheffield,S1 1WB, England, UK

[‡]Department of Mathematics, Sri Venkateswara University, Tirupati-517502

Nomenclature

x, y	coordinates along the cone generator and normal to the generator;	U, V	dimensionless velocity components along the X- and Y-directions
u, v	velocity components along the x- and y-directions	b	Forchheimer geometrical constant
g	gravitational acceleration	Da	Darcy number
r	local radius of cone	Fs	Forchheimer number
t'	time	Gr_L	Grashof number
t	dimensionless time	M	magnetic parameter
T'	temperature	B_0	magnetic field strength
T	dimensionless temperature	Pr	Prandtl number
C'	concentration	N	buoyancy ratio parameter
C	dimensionless concentration	Sc	Schmidt number
D	mass diffusion coefficient	m	power-law index for surface heat flux relation
K	permeability of porous medium		
q_w	heat flux (i.e. heat transfer rate per unit area)	n	power-law index for surface mass flux relation
q_w^*	mass flux (i.e. mass transfer rate per unit area)	Nu_x	local Nusselt number
k	thermal conductivity of fluid	Nu_X	dimensionless local Nusselt number
L	reference length	Sh_x	local Sherwood number
X, Y	dimensionless coordinates along the cone generator and normal to the generator	Sh_X	non-dimensional local Sherwood number
		R	dimensionless local radius of cone

Greek symbols

μ	dynamic viscosity of fluid		cient
ν	kinematic viscosity of fluid	θ	dimensionless temperature function
ϕ	semi-vertical cone angle	τ	dimensionless time
α	thermal diffusivity	τ_X	dimensionless local shear stress function (skin friction)
β	volumetric thermal expansion coeffi-		

Subscripts

w	condition on the wall	∞	free stream condition

1   Introduction

Combined heat and mass transfer in fluid-saturated porous media finds applications in a variety of engineering processes such as heat exchanger devices,

petroleum reservoirs, chemical catalytic reactors and processes and others. A thorough discussion of these and other applications is available in the monographs by Ingham and Pop [11] and Nield and Bejan [13]. Comprehensive reviews of the much of the work communicated in porous media transport phenomena have been presented by Vafai [16] and Trevisan and Bejan [14]. Most studies dealing with porous media have employed the Darcy law. However, for high velocity flow situations, the Darcy law is inapplicable, since it does not account for inertial effects in the porous medium. Such flows can arise for example in the near-wellbore region of high capacity gas and condensate petroleum reservoirs and also in highly porous filtration systems under high blowing rates. The most popular approach for simulating high-velocity transport in porous media is the Darcy–Forchheimer drag force model. This adds a second-order (quadratic) drag force to the momentum transport equation. This term is related to the geometrical features of the porous medium and is independent of viscosity. Vafai and Tien [15] presented a seminal study discussing the influence of Forchheimer inertial effects in porous media convection. Chen and Chen [4] studied the mixed convective boundary layer flow from a vertical surface in a fluid-saturated non-Darcian porous medium including Forchheimer inertial effects. Hossain and Paul [10] studied thermal convection boundary layer flow with buoyancy and suction/blowing effects from a cone with non-uniform surface temperature. They extended this study [9] to consider non-uniform surface heat flux, both studies employing numerical methods. Chamkha et al. [3] studied the double-diffusive convection heat and mass transfer over a cone (and wedge) in Darcy-Forchheimer porous media. Magnetohydrodynamic (MHD) flow and heat transfer is of considerable interest because it can occur in many geothermal, geophysical, technological, and engineering applications such as nuclear reactors and others. The geothermal gases are electrically conducting and are affected by the presence of a magnetic field. Vajravelu and Nayfeh[17] studied hydromagnetic convection from a cone and a wedge with variable surface temperature and internal heat generation or absorption. Thusfar the transient thermal convection flow over a cone in Darcy-Forchheimer porous media has not been studied in the literature despite important applications in geothermics, geophysics and materials processing.

2 Mathematical model

An axisymmetric unsteady natural convection boundary layer flow past a vertical cone with transverse magnetic field applied normal to the surface with

variable heat and mass flux in a Darcy-Forchheimer fluid saturated porous medium in a cartesian (x, y) coordinate system is formulated mathematically in this section. Initially, it is assumed that the cone surface and the surrounding fluid which are at rest possess the same temperature T'_∞ and concentration level C'_∞ everywhere in the fluid. At time $t' > 0$, heat supplied from the cone surface to the fluid, concentration level near the cone surface are raised at a rate of $q_w(x) = x^m$ and $q^*_w(x) = x^n$ respectively, and they are maintained at the same level. It is assumed that the concentration C' of the diffusing species in the binary mixture is very less in comparison to the other chemical species, which are present and hence the Soret and Dufour effects are negligible. We consider viscous flow where pressure work, viscous dissipation and thermal dispersion effects are neglected.
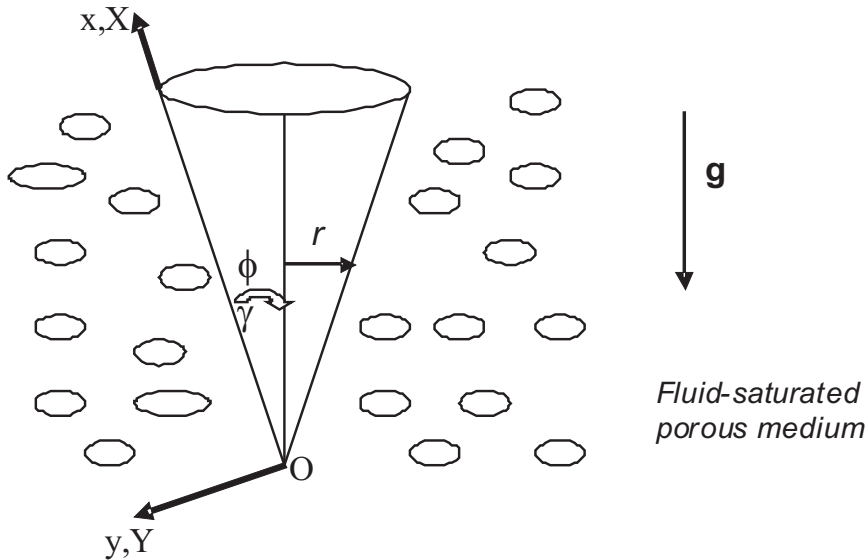

Figure 1: Physical Model

The coordinate system chosen (as shown in Fig.1) is such that the x-direction is measured along the cone surface from the leading edge O, and the y-direction is normal to the cone generator. The cone apex is located at the origin (x=y=0).

Here φ designates the semi-vertical angle of the cone and r is the local

radius of the cone.

Then under the above assumptions, the governing boundary layer equations with Boussinesq's approximation are

$$\frac{\partial (ur)}{\partial x} + \frac{\partial (vr)}{\partial y} = 0 \tag{1}$$

$$\frac{\partial u}{\partial t'} + u\frac{\partial u}{\partial x} + v\frac{\partial u}{\partial y} = \nu\frac{\partial^2 u}{\partial y^2} - \frac{\sigma B_0^2}{\rho}u + g\beta\cos\varphi(T' - T'_\infty)$$

$$+ g\beta^*\cos\varphi(C' - C'_\infty) - \frac{\nu}{K}u - \frac{b}{K}u^2 \tag{2}$$

$$\frac{\partial T'}{\partial t'} + u\frac{\partial T'}{\partial x} + v\frac{\partial T'}{\partial y} = \alpha\frac{\partial^2 T'}{\partial y^2} \tag{3}$$

$$\frac{\partial C'}{\partial t'} + u\frac{\partial C'}{\partial x} + v\frac{\partial C'}{\partial y} = D\frac{\partial^2 C'}{\partial y^2} \tag{4}$$

where all terms are defined in the nomenclature. Under the Boussinesq approximation buoyancy effects are simulated only in the momentum equation, which is coupled to the energy equation, constituting a free convection regime. The corresponding spatial and temporal initial and boundary conditions at the surface and far from the cone take the form:

$$t' \leq 0 : u = 0, \, v = 0, T' = T'_\infty, \, C' = C'_\infty \quad for \, all \, x, y,$$

$$t' > 0 : \, u = 0, \, v = 0, \, \frac{\partial T'}{\partial y} = -\frac{q_w(x)}{k}, \, \frac{\partial C'}{\partial y} = -\frac{q_w^*(x)}{D} \quad at \, y = 0,$$

$$u \to 0, \, T' \to T'_\infty, \, C' \to C'_\infty \quad at \, x = 0, \tag{5}$$

$$u \to 0, \, T' \to T'_\infty, \, C' \to C'_\infty \quad as \, y \to \infty.$$

where all the parameters defined in the nomenclature.

The equations (1) to (4) are highly coupled, parabolic and nonlinear. An analytical solution is clearly intractable and in order to facilitate a numerical solution we *non-dimensionalize* the model. Proceeding with the analysis we now introduce the following transformations:

$$X = \frac{x}{L}, \quad Y = \frac{y}{L}(Gr_L)^{\frac{1}{4}}, \quad R = \frac{r}{L}, \quad where \, r = x\sin\varphi,$$

$$V = \frac{vL}{\nu}(Gr_L)^{-\frac{1}{4}}, \quad U = \frac{uL}{\nu}(Gr_L)^{-\frac{1}{2}}, \quad t = \frac{\nu t'}{L^2}(Gr_L)^{\frac{1}{2}} \quad M = \frac{\sigma B_0^2 L^2}{\mu}Gr_L^{-\frac{1}{2}} \tag{6}$$

$$T = \frac{T' - T'_\infty}{[q_w(L)L/k]}, \quad Gr_L = \frac{g\beta \cos\phi[q_w L/k]L^4}{\nu^2}, \quad \Pr = \frac{\nu}{\alpha}, \quad Da = \frac{K}{L^2}$$

$$C = \frac{C' - C'_\infty}{[q_w^*(L)L/D]}, \quad N = \frac{\beta^*(C'_w - C'_\infty)}{\beta(T'_w - T'_\infty)}, \quad Sc = \frac{\nu}{D}, \quad Fs = \frac{b}{L}$$

The transport equations (1) to (4) are thereby reduced to the following dimensionless form

$$\frac{\partial(UR)}{\partial X} + \frac{\partial(VR)}{\partial Y} = 0 \tag{7}$$

$$\frac{\partial U}{\partial t} + U\frac{\partial U}{\partial X} + V\frac{\partial U}{\partial Y} = \frac{\partial^2 U}{\partial Y^2} - MU + T\cos\varphi + NC\cos\varphi - \frac{U}{DaGr_L} - \frac{Fs}{Da}U^2 \tag{8}$$

$$\frac{\partial T}{\partial t} + U\frac{\partial T}{\partial X} + V\frac{\partial T}{\partial Y} = \frac{1}{\Pr}\frac{\partial^2 T}{\partial Y^2} \tag{9}$$

$$\frac{\partial C}{\partial t} + U\frac{\partial C}{\partial X} + V\frac{\partial C}{\partial Y} = \frac{1}{Sc}\frac{\partial^2 C}{\partial Y^2} \tag{10}$$

The corresponding non-dimensional initial and boundary conditions are given by

$$t \leq 0 : U = 0, \ V = 0, \ T = 0, \ C = 0 \quad for \ all \ X, Y,$$

$$t > 0 : U = 0, \ V = 0, \ \frac{\partial T}{\partial Y} = -X^m, \frac{\partial C}{\partial Y} = -X^n \quad at \ Y = 0, \tag{11}$$

$$U = 0, \quad T = 0, \quad C = 0 \quad at \ X = 0,$$

$$U \to 0, \quad T \to 0, \quad C \to 0 \quad as \ Y \to \infty,$$

where again all the parameters are given in the nomenclature. The dimensionless local values of the skin friction, Nusselt number and the Sherwood number are given by the following expressions

$$\tau_x = -\left(\frac{\partial U}{\partial Y}\right)_{Y=0} \tag{12}$$

$$Nu_x = -X\left(\frac{\partial T}{\partial Y}\right)_{Y=0} \tag{13}$$

$$Sh_x = -X\left(\frac{\partial C}{\partial Y}\right)_{Y=0} \tag{14}$$

3 Numerical solution

In order to solve the unsteady, non-linear, coupled equations (7) – (10) under the conditions (11), an implicit finite difference scheme of Crank-Nicolson type has been employed which is discussed by many authors Muthu-cumaraswamy and Ganesan [12], Gouse Mohiddin [6] and Gouse Mohiddin *et al* [7] and Bapuji et al. [1]. The finite difference scheme of dimensionless governing equations is reduced to tri-diagonal system of equations and is solved by Thomas algorithm as discussed in Carnahan et al. [2]. The region of integration is considered as a rectangle with $X_{\max} = 1$ and $Y_{\max} = 22$ where $Y_{\max}$ corresponds to $Y = \infty$ which lies very well out side both the momentum and thermal boundary layers. The maximum of Y was chosen as 22, after some preliminary investigation so that the last two boundary conditions of (11) are satisfied within the tolerance limit 10^{-5}. The mesh sizes have been fixed as $\Delta X = 0.05, \Delta Y = 0.05$ with time step $\Delta t = 0.01$. The computations are carried out first by reducing the spatial mesh sizes by 50% in one direction, and later in both directions by 50%. The results are compared. It is observed in all cases, that the results differ only in the fifth decimal place. Hence, the choice of the mesh sizes seems to be appropriate. The scheme is unconditionally stable. The local truncation error is $O(\Delta t^2 + \Delta Y^2 + \Delta X)$ and it tends to zero as $\Delta t, \Delta X$ and ΔY tend to zero. Hence, the scheme is compatible. Stability and compatibility ensure the convergence. The derivatives involved in Equations (12) – (14) are evaluated using five point approximation formula.

4 Results and discussion

Only selective figures have been reproduced here for brevity. In the numerical computations the following values for the dimensionless thermophysical parameters are prescribed: Grashof number $(Gr_L) = 1.0$, Darcy number (Da) = 0.1 (high permeability), Forchheimer number (Fs) = 0.1 (weak quadratic drag), Prandtl number (Pr) = 7.0 (water), Schmidt number (Sc) = 0.6 (oxygen diffusing in air), surface heat flux power law exponent (m) = 0.5, surface mass flux power law exponent (n) = 0.5, buoyancy ratio parameter (N) = 1.0 and semi-vertical angle of the cone $(\varphi) = 20^0$. All graphs therefore correspond to these values unless otherwise indicated. To test the accuracy of the computations the local shear stress and local Nusselt number computations for the non-porous case are compared with those of Hossain and Paul [9] for a heat flux gradient of m = 0.5 and X = 1.0 in the steady state, in Tables 1, 2 respectively, and are found to be in good agreement.

Table 1: Comparison of local skin friction values at X = 1.0 and m = 0.5 with those of Hossain-Paul [9] for steady state purely fluid ($Da \to \infty$ in present model) case.

| Pr	Hossain and Paul [9] $\Gamma_X/Gr_L^{3/5}$	Present results
0.01	5.13457	5.13424
0.05	2.93993	2.93180
0.1	2.29051	2.29044

Table 2: Comparison of local Nusselt number values at X = 1.0 and m = 0.5 with those of Hossain-Paul [9] for steady state purely fluid (Da $\to \infty$ in present model) case.

Pr	Hossain and Paul [9] $Nu_X/Gr_L^{3/5}$	Present results
0.01	0.14633	0.14648
0.05	0.26212	0.26227
0.1	0.33174	0.33648

In Figures 2(a) and 2(b), the influence of Grashof number (Gr_l) on steady state velocity(U) and temperature (T) distributions with Y-coordinate are shown. Free convection i.e. thermal buoyancy effects are analyzed via the Grashof number. For an increasing Gr_l from 0.1 through 1.0, 10.0, 50.0 to 100.0 cooling of the cone by free convection occurs i.e. heat is conducted away from the cone to the surrounding regime.

Figures 2(a) and 2(b) show the effect of Darcy number (Da) on dimensionless velocity (U) and temperature (T) with transformed radial coordinate (Y) close to the leading edge (i.e. cone apex) at X = 1.0. To study the influence of regime permeability from sparsely packed media to densely packed materials the following values Da = 1.0, 0.1, 0.01, 0.001 are considered. Da $= K/L^2$ for a fixed value of the reference length (L) is directly proportional to permeability (K) of the porous regime. Increasing Da increases the porous medium permeability and simultaneously decreases the Darcian impedance since progressively less solid fibers are present in the regime. The flow is
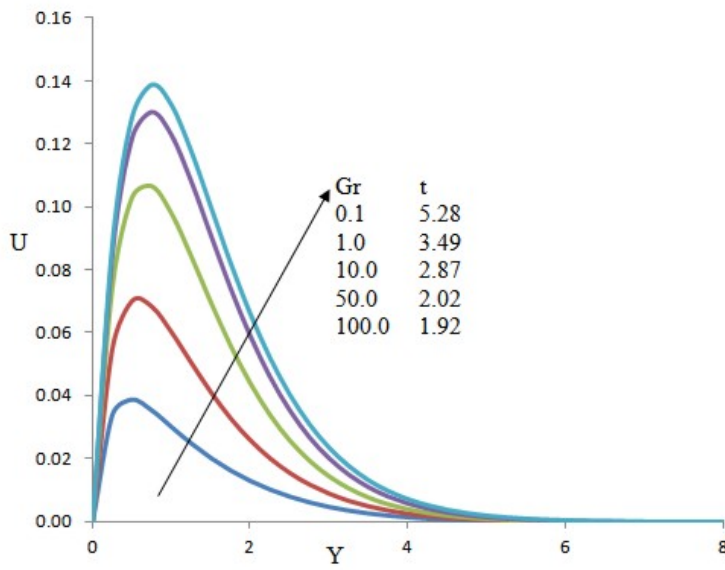
(a) Velocity profiles
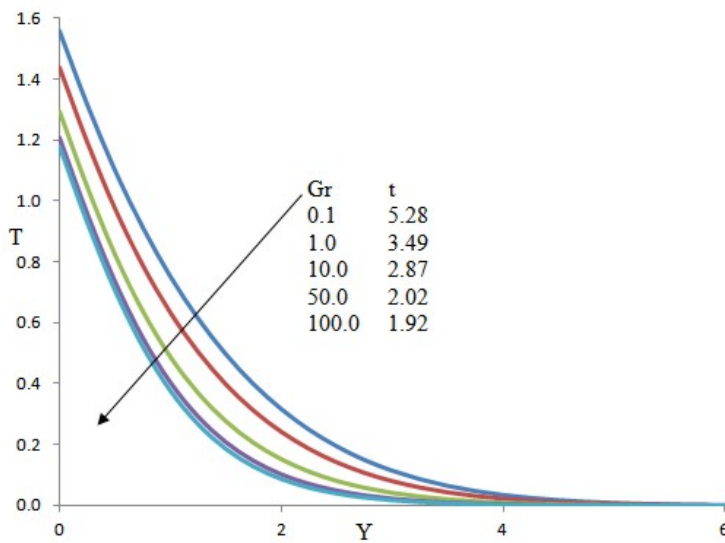
(b) temperature profiles

Figure 2: Steady state velocity and temperature profiles at X=1.0 for different Gr

therefore accelerated for higher Da values causing an increase in the velocity U as shown in Figure 2(a). Maximum effect of rising Darcy number is observed at intermediate distance from the cone surface around Y ∼ 1. Conversely temperature T depicted in Figure 2(b) is opposed by increasing Darcy number. The presence of fewer solid fibers in the regime with increasing Da inhibits the thermal conduction in the medium which reduces distribution of thermal energy. The regime is therefore cooled when more fluid is present and T values in the thermal boundary layer are decreased. Profiles for both velocity and temperature are smoothly asymptotic decays to the free stream indicating that excellent convergence (and stability) is obtained with the numerical method. Velocity boundary layer thickness will be increased with a rise in Da and thermal boundary layer thickness reduced.

The effect of the Forchheimer inertial drag parameter (Fs) on dimensionless temperature (T) profiles is shown in Figure 3.

The Forchheimer drag force is a second order retarding force simulated in the momentum conservation equation. Increasing Fs values from 0.0 through 0.1,1.0,5.0,10.0,20.0 and 50.0 causes a strong increase in Forchheimer drag which decelerates the flow i.e. reduces velocities. For higher values of Fs it is expected that the porous medium flow becomes increasingly chaotic. Temperature (T) however is slightly increased with a rise in Forchheimer parameter. The effects of the Prandtl number (Pr) on velocity profiles are depicted in Figure 4.

Pr encapsulates the ratio of momentum diffusivity to thermal diffusivity. Larger Pr values imply a thinner thermal boundary layer thickness and more uniform temperature distributions across the boundary layer. Hence thermal boundary layer will be much less thick than the hydrodynamic (translational velocity) boundary layer. Smaller Pr fluids have higher thermal conductivities, so that heat can diffuse away from the cone surface faster than for higher Pr fluids (thicker boundary layers). Physically the lower values of Pr correspond to liquid metals (Pr ∼ 0.02, 0.05), Pr = 0.7 is accurate for air or hydrogen and Pr = 7.0 for water. The computations show that translational velocity U is therefore reduced as Pr rises from 0.72 through 1.0, 2.0, 5.0, 7.0 and 10.0 since the fluid is increasingly viscous as Pr rises. Figure 4(b) indicates that a rise in Pr substantially reduces the temperature T in saturated porous regime.

The profiles become increasingly parabolic as Pr increases above 0.1, for which the profile is approximately a linear decay. For all cases T decays to
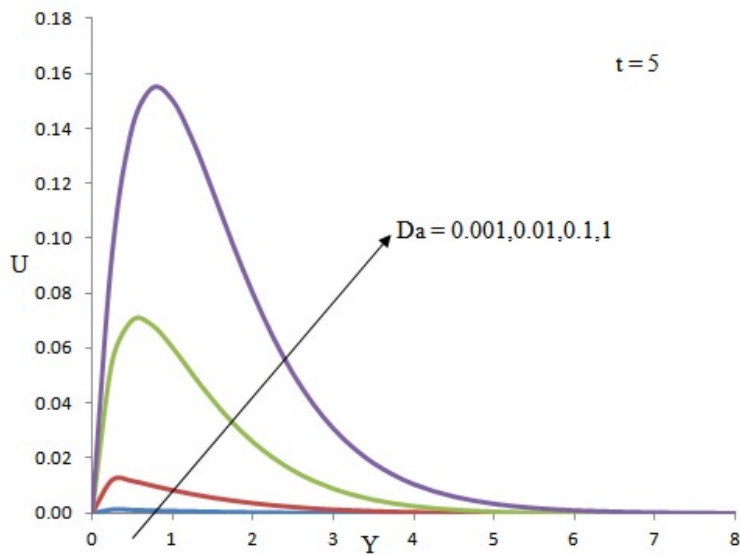
(a) Transient velocity profiles
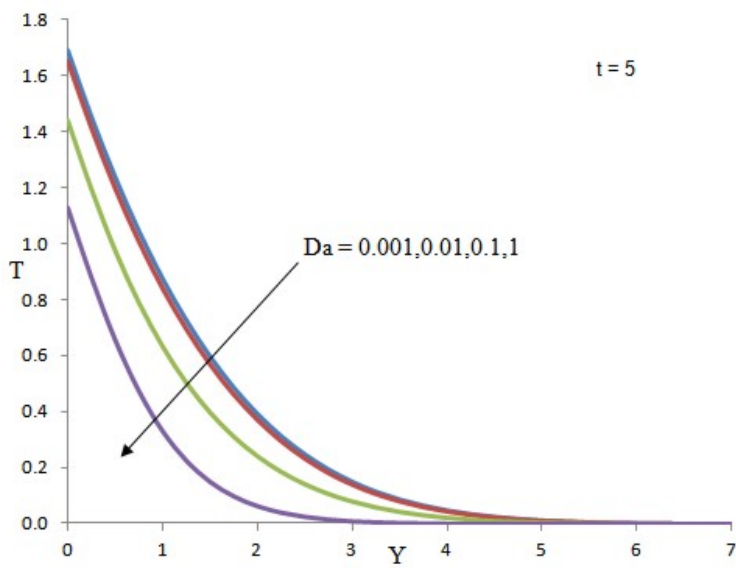
(b) Transient temperature profiles

Figure 3: Transient velocity and temperature profiles at X=1.0 for different Da

zero as $Y \rightarrow \infty$, i.e. in the free stream. There is however a rapid decay to zero for the maximum Pr ($= 10$) where the temperature plummets to zero in the near-wall region. Concentration function values are seen to increase slightly with an increase in Pr.
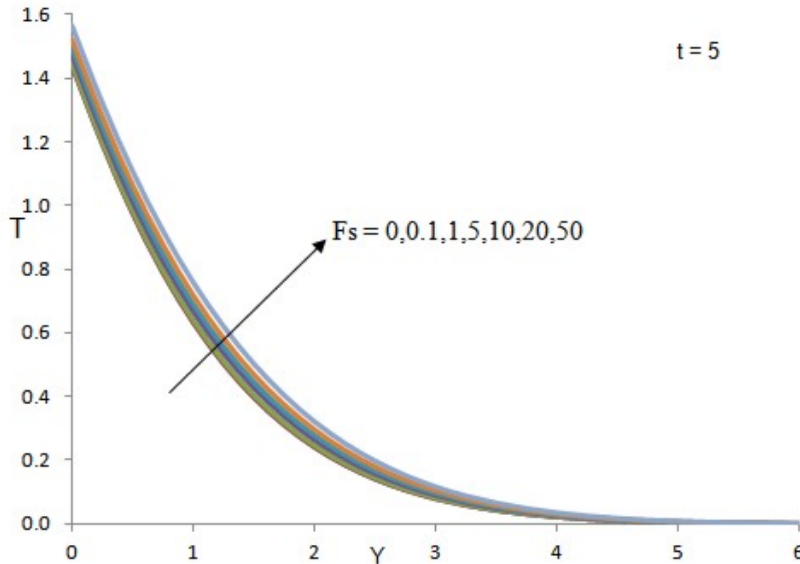

Figure 4: Transient temperature profiles at X=1.0 for different Fs

Figure 5 shows the effect of the Schmidt number (Sc) on the dimensionless concentration (C).

We note that the Schmidt number (Sc) embodies the ratio of the momentum to the mass diffusivity. Sc therefore quantifies the relative effectiveness of momentum and mass transport by diffusion in the hydrodynamic (velocity) and concentration (species) boundary layers. Smaller Sc values can represent for example hydrogen gas as the species diffusing in air , Sc $= 2.0$ implies hydrocarbon diffusing in air, and higher values to petroleum derivatives diffusing in fluids (e.g. ethyl benzene) as indicated by Gebhart et al. [8]. As Sc increases, Figure 5 shows that C values are strongly decreased, as larger values of Sc correspond to a decrease in the chemical molecular diffusing i.e. less diffusion therefore takes place by mass transport. The dimensionless concentration profiles all decay from a maximum concentration to zero in the freestream. Greater Sc values correspond to lower chemical molecular diffusivity of the parent fluid so that less diffusion of the species occurs in the

regime. Concentration boundary layer thickness will therefore be reduced. For low Sc fluid greater species diffusion occurs and concentration boundary layer thickness increased. For Sc = 1, the Concentration and velocity boundary layers will have approximately the same thickness i.e. species and momentum will be diffused at the same rates. With lower Sc values the decay of concentration from the cone surface is more controlled, for increasing values of Sc the profiles descend more and more steeply and concentration falls faster from the surface to a short distance into the boundary layer regime.
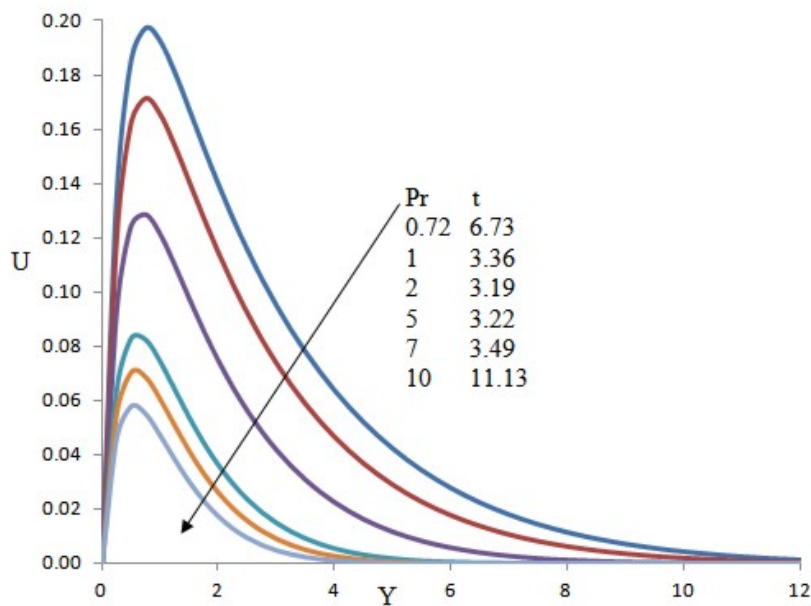
Figure 5: Transient temperature profiles at X=1.0 for different Pr

The effect of surface heat flux power exponent (m) on the steady state temperature (T) is shown in Figure 6.

An increase in the value of m reduces the temperature. It is also seen that the time required to reach the steady state temperature is more at lower values of m. Figure 7 depict the distribution of concentration (C) with radial coordinate (Y) for various values of the surface mass flux power law exponent (n).

The concentration reduces with the increasing n values from 0.0 through 0.25, 0.50, 0.75 and 1.0.

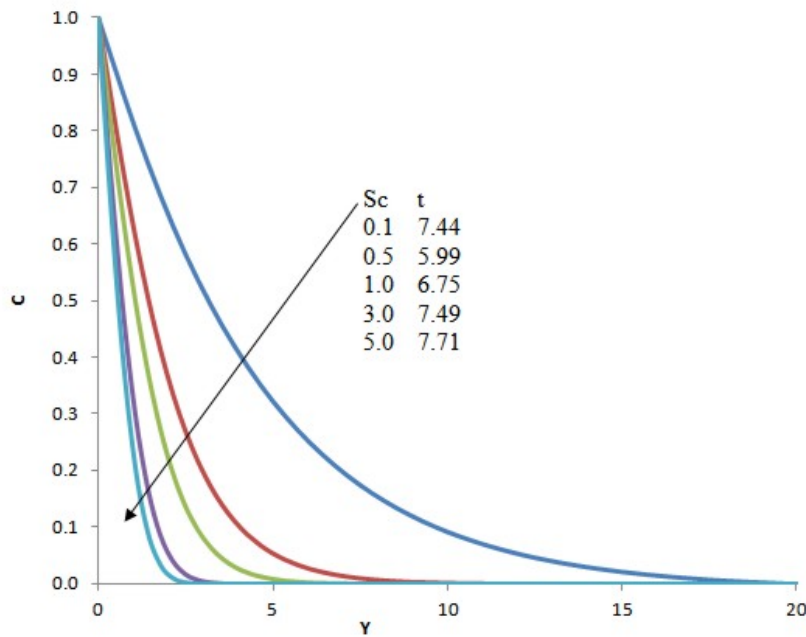Increasing Fs clearly reduces the local Nusselt number as shown in Fig.8.

Figure 6: Steady state concentration profiles at X=1.0 for different Sc

N = 0 indicates that thermal and species buoyancy forces are both absent. For $N > 0$, thermal and species buoyancy forces aid each other. N = 1 implies that both buoyancy forces are of the same order of magnitude. A rise in N from 0.0 through 1.0, 2.0, 3.0 and 5.0 induces a retarding effect on the flow in the porous regime i.e. velocities are decreased. Increasing N (thermal and concentration buoyancy forces assisting each other) decreases temperatures in the regime i.e. cools the boundary layer regime. The effect of semi-vertical angle of the cone (ϕ) on dimensionless temperature (T) with Y-coordinate is shown in Figure 11.

A slight increase in local Nusselt number accompanies the increment in Pr as shown in Figure 10.

The influence of the concentration to thermal buoyancy ratio parameter (N), on dimensionless temperature (T) with radial coordinate (Y) is shown in Figure 10.
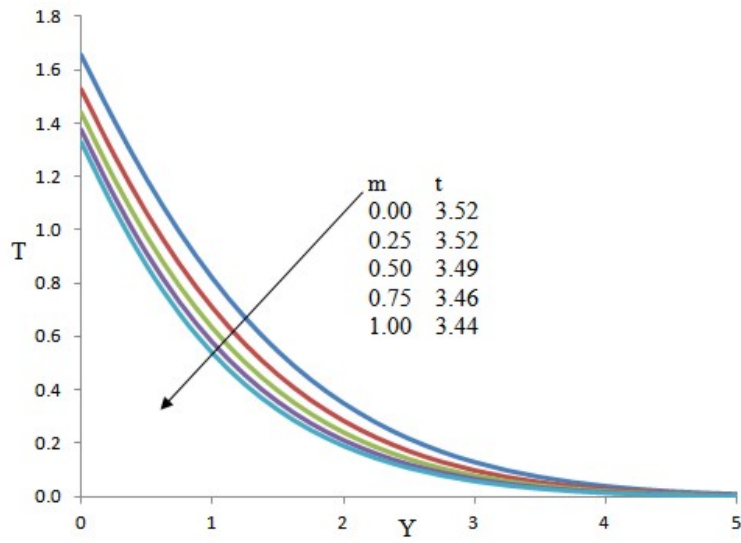
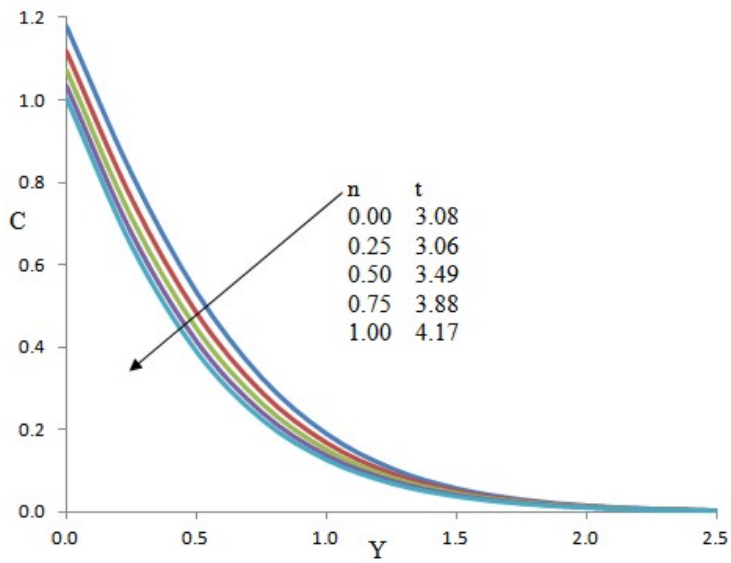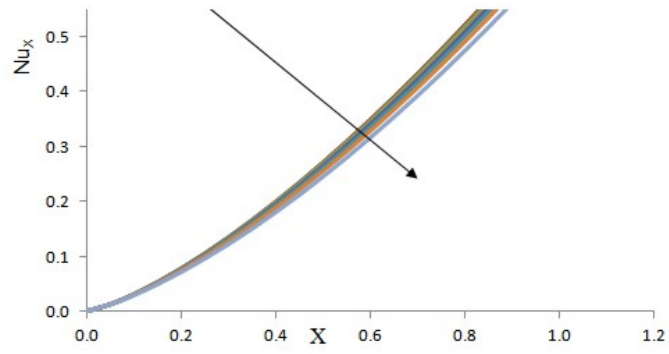Figure 7: Steady state temperature profiles at X=1.0 for different Sc
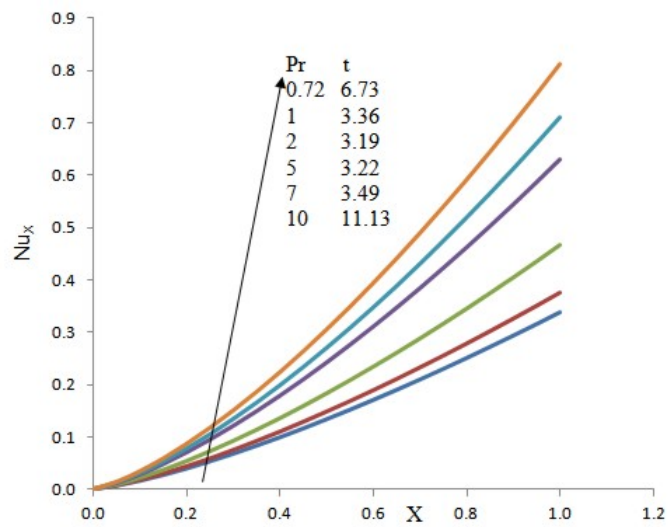

Figure 8: Steady state concentration profiles at X=1.0 for different n

Figure 9: Effect of Fs on local Nusselt number at X=1.0
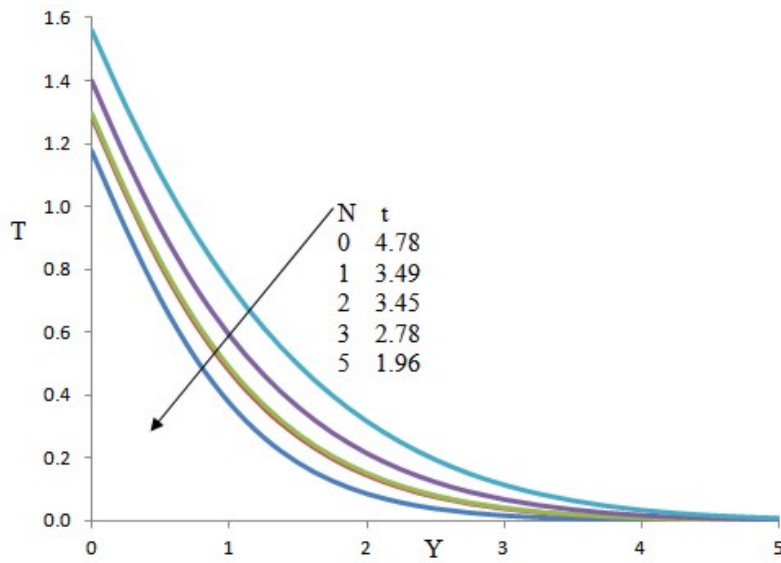

Figure 10: Effect of Pr on local Nusselt number at X=1.0

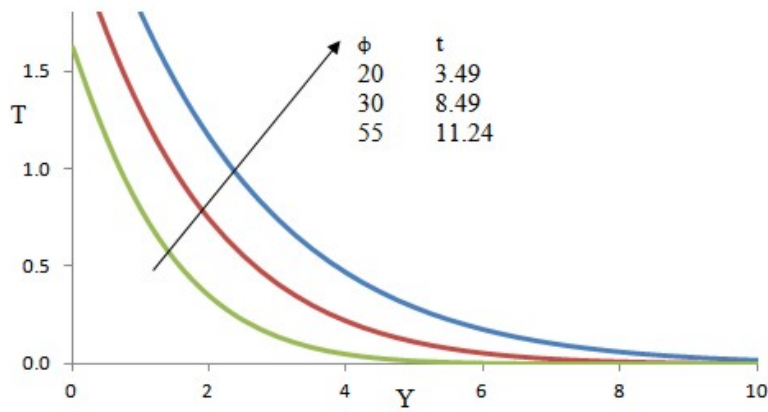Figure 11: Steady state temperature profiles at X=1.0 for different N

Figure 12: Steady state temperature profiles at X=1.0 for different φ

It is observed that a rise in ϕ substantially increases the temperature T in the boundary layer regime. And more time is required to reach the steady state. Figures 12 the influence of magnetic parameter (M) versus spanwise spatial distributions of velocity U are depicted.

Application of magnetic field normal to the flow of an electrically conducting fluid gives rise to a resistive force that acts in the direction opposite to that of the flow. This force is called the Lorentz force. This resistive force tends to slow down the motion of the fluid along the cone and causes an increase in its temperature and a decrease in velocity as M increases. An increase in M from 1 though 2, 3, 4 clearly reduces streamwise velocity U both in the near-wall regime and far-field regime of the boundary layer.
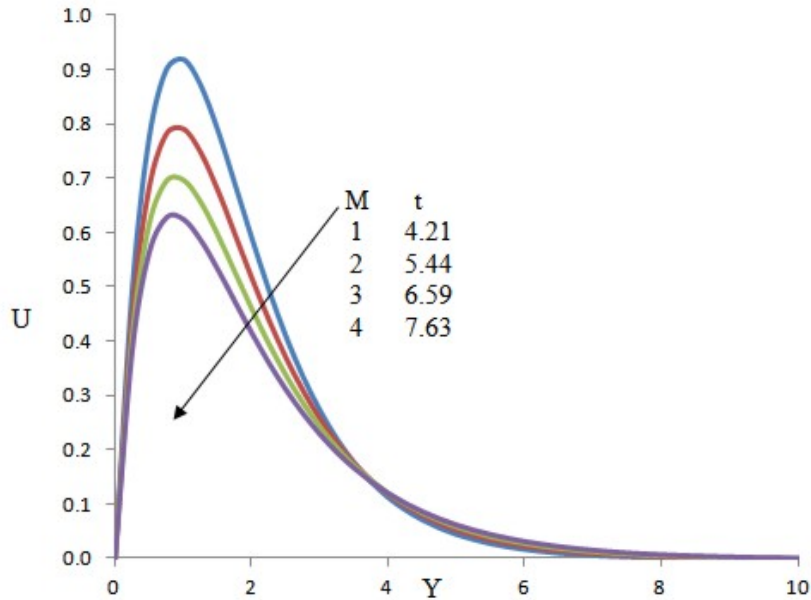

Figure 13: Steady state velocity profiles at X=1.0 for different values of M

5 Conclusions

Numerical solutions have been presented for the buoyancy-driven unsteady natural convection boundary layer flow past a vertical cone embedded in a non Darcian isotropic porous regime. Present results are compared with those of Hossain and Paul [9] and found to be in excellent agreement. The following

conclusions are drawn.

- Increasing Grashof number boosts the translational velocity in the cone surface regime and decreases temperature throughout the flow regime.

- Increasing Darcy number accelerates the flow i.e. increases translational velocities. However the temperature is reduced with a rise in Darcy number.

- An increase in the Forchheimer inertial drag parameter is observed to slightly increase the temperature, but reduces both velocity and local Nusselt number.

- An increase in Prandtl number is observed to decrease both temperature and velocity, but the concentration is slightly increased. A slight increase in local Nusselt number accompanies the increment in Pr.

- The concentration is observed to significantly decrease with an increase in Schmidt number.

- The temperature is observed to decrease with an increase in buoyancy ratio parameter, but decrease with an increase in semi-vertical angle of the cone. The time taken to reach the steady state increases with increasing ϕ.

References

[1] Bapuji Pullepu, Ekambavanan, K., Chamkha, A. J., Unsteady laminar free convection from a vertical cone with uniform surface heat flux, Nonlinear Analysis: Modelling and Control., 13 (2008) 47-60.

[2] Carnahan, B., Luther, H. A., Wilkes, J.O., Applied Numerical Methods, John Wiley and Sons, New York (1969).

[3] Chamkha, A.J., Khalid, A. R. A., Al-Hawaj, O., Simultaneous Heat and Mass Transfer by Natural Convection from a Cone and a Wedge in Porous Media, J. Porous Media, 3 (2000) 155-164.

[4] Chen, C. H., Chen, C. K., Non-Darcian mixed convection along a vertical plate embedded in a porous medium, Applied Mathematical Modelling, 14 (1990) 482-488.

[5] Chen, C. K., Chen, C. H., Minkowycz, W. J., Gill, U. S., Non-Darcian effects on mixed convection about a vertical cylinder embedded in a saturated porous medium, Int. J. Heat Mass Transfer, 35 (1992) 3041-3046.

[6] Gouse Mohiddin, S., Computational Fluid Dynamics, LAP Lambert Academic Publishing, Germany 2011.

[7] Gouse Mohiddin, S., Prasad, V. R., Varma, S. V. K., Anwar Bég, O., Numerical Study Of Unsteady Free Convective Heat And Mass Transfer In A Walters-B Viscoelastic Flow Along A Vertical Cone, Int. J. of Appl. Math. and Mech., 6 (2010) 88-114.

[8] Gebhart, B., Jaluria, Y., Mahajan, R.L., Sammakia, B., Buoyancy – Induced flows and Transport, Hemisphere, New York 1998.

[9] Hossain, M.A., Paul, S.C., Free convection from a vertical permeable circular cone with non-uniform surface heat flux, Heat Mass Transfer, 37 (2001) 167-173.

[10] Hossain, M.A., Paul, S.C., Free convection from a vertical permeable cone with non-uniform surface temperature, Acta Mechanica, 151 (2001) 103-114.

[11] Ingham, D. B., Pop, I., Transport Phenomena in Porous Media II, Pergamon, Oxford (2002).

[12] Muthucumaraswamy, R., Ganesan, P., Unsteady flow past an impulsively started vertical plate with heat and mass transfer, Heat Mass Transf., 34 (1998) 187-193.

[13] Nield, D. A., Bejan, A., Convection in Porous Media, 3-rd edition, Springer, New York (2006).

[14] Trevisan, O. V., Bejan, A., Combined heat and mass transfer by natural convection in a porous medium, Adv. Heat Transfer, 20 (1990) 315-352.

[15] Vafai, K., Tien, C. L., Boundary and inertia effects on flow and heat transfer in porous media, Int.J. Heat Mass Transfer, 24 (1981) 195-203.

[16] Vafai, K. (Ed.), Handbook of Porous Media, 2-nd edition, CRC Press, Boca Raton (2005).

[17] Vajravelu, K., Nayfeh, L., Hydromagnetic convection at a cone and a wedge, Int Commun Heat Mass Transfer, 19 (1992) 701-710.

Submitted in September 2013.

Numerička studija slobodnog konvektivnog MHD tečenja preko vertikalne kupe u nedarsiskoj poroznoj sredini

Izvedena je numerička studija nestacionarne prirodne konvekcije potiskom izazvanog graničnog sloja pri strujanju oko vertikalne kupe u nedarsijskom izotropnom poroznom režimu sa poprečnim magnetnim poljem primenjenim normalno na površ. Protok toplote i mase na površi membrane kupe se modelira kao stepeni red u skladu sa $q_w(x) = x^m$ kao i $q_w^*(x) = x^n$, po redu, gde x oznacava koordinatu duž nagnute strane kupe. Darsijski otpor i Forhajmerova impedanca kvadratne poroznosti su obe uključeni u dvomerni viskozni model tečenja. Jednačine prelaznog graničnog sloja su tada prevedene u bezdimenzioni oblik rešene implicitnom Crank-Nicolson metodom konačnih razlika. Uticaji Grashofovog broja, Darcijevog broja, Forchajmerovog broja, Prandtlovog broja, stepenog eksponenta (m) površine toplotnog protoka, stepenog eksponenta (n) površinskog protoka mase, Šmitovog broja, parametra odnosa potiska i vertikalnog polu-ugla kupe na polja brzine, temperature i koncentracije su proučeni. Ovi rezultati za odabrane promenljive varijabli u režimu čisto fluidnom su poredjeni sa studijom ne-poroznosti Hosaina i Pula [9] i nadjeno je da su u odlicnoj saglasnosti. Lokalno trenje na zidu, Nuseltov broj i Šervudov broj su takode analizirani grafički. Studija nalazi važne primene u geofizičom prenosu toplote, industrijskim proizvodnim procesima i hibridnim solarnim energetskim sistemima.